Thermoelectric and Spin-caloritronic Coolers: From Basics to Recent Developments

Joseph P. Heremans[1,2,3] and Hyungyu Jin[4]

1. Department of Mechanical and Aerospace Engineering, The Ohio State University, Columbus, Ohio 43210

2. Department of Materials Science and Engineering, The Ohio State University, Columbus, Ohio 43210

3. Department of Physics, The Ohio State University, Columbus, Ohio 43210

4. Department of Mechanical Engineering, Stanford University, Stanford, California 94305

ABSTRACT

Solid-state coolers have no moving parts, and are therefore compact, vibration-free, inherently durable, and scalable to low power levels. Unfortunately, they have a low coefficient of performance. The materials characteristic that sets this efficiency in solid-state coolers is the thermoelectric figure of merit, zT.

This article reviews the factors limiting zT in conventional thermoelectric devices, then outlines modern approaches to increasing zT. It describes a new solid-state energy conversion technology, the spin-Seebeck effect (SSE). New concepts are outlined that combine classical thermoelectric and SSE physics. By exploiting the spin degree of freedom, we hope to increase the performance of solid-state coolers.

KEY WORDS: Thermoelectrics, Spin-Seebeck effect, Solid state cooling, Magnon-drag

1. INTRODUCTION

Historically, cryogenic cooling down to 10 K and below has been provided by either thermodynamic cycles or by stored cryogens. If all-solid-state cooling could be achieved, via for example the Peltier effect, it would have several technological advantages. The absence of moving parts in thermoelectric coolers make the devices vibration-free, maintenance-free, and, if properly designed, completely reliable with an essentially infinite lifetime. Thermoelectric devices have also an extremely high specific cooling capacity. However, this property depends more on the heat exchanger design than on the actual Peltier cooling material itself because the latter constitutes only a small fraction of the volume of the cooler. An additional potential benefit of the high density is an intrinsically short response time because no fluid needs to be condensed. The inherent drawbacks of thermoelectric devices are their low coefficient of performance, which is entirely limited by irreversible heat losses.

We are aware of the potential of pseudo-solid-state cooling technologies, such as magneto-caloric cooling, which still need the use of variable heat exchangers. This in turn implies that they have to use either mechanical actuators or variable magnetic fields. Pure solid-state devices are based on the Peltier, Nernst-Ettingshausen, transverse Peltier, and spin-Seebeck related effects, and they will be reviewed here. They, or hybrids between them, offer the greatest potential for advances to bring their operating temperature range down to 10 K from ~170 K, which is the temperature achievable today with commercial six-stage Peltier coolers.

Optical and Electronic Cooling of Solids, edited by Richard I. Epstein, Denis V. Seletskiy, Mansoor Sheik-Bahae, Proc. of SPIE Vol. 9765, 976507 · © 2016 SPIE
CCC code: 0277-786X/16/$18 · doi: 10.1117/12.2208541

2. PELTIER COOLERS

When a solid is subjected to a temperature gradient (∇T), a heat flux (j_Q) flows through it. To the first order, the heat flux is linearly related to ∇T via Fourier's law, $j_Q = \kappa \nabla T$, where κ is the solid's thermal conductivity. Both ∇T and j_Q are vectors; in the absence of external magnetic fields they are collinear. When the solid is electrically conducting (metals or semiconductors), ∇T also generates an electric field E, again aligned with ∇T in the absence of an external magnetic field. In linear transport theory, E and ∇T are proportional to each other. The thermoelectric power α of the solid, also known as thermopower or Seebeck coefficient, is the proportionality constant, defined as $\alpha \equiv E/\nabla T$. By the Onsager reciprocity relation[1], applying an electrical current I to the material creates a heat pumping action, generating a heat flow Q in the material linearly proportional to I, with a proportionality constant Π, called the Peltier coefficient: $Q = \Pi I$. This Peltier coefficient is related to the thermopower α by the Onsager relation[1] $\Pi = \alpha T$, which is based on the second principle of thermodynamics. It has been shown by Callen[1] that, for a single electron and in strictly reversible thermodynamics, the thermopower equals the entropy S of that electron divided by its charge e, $\alpha = S/e$. Consequently:

1. The thermopower is a state equation: it does not matter how the electron goes from point A to B in a sample, just what the potential and temperature are at points A and B;
2. The thermopower is an absolute property of a material, not a difference. It does not require a thermocouple made from two materials to measure a thermopower. The absolute value of thermopower is measured by calorimetry by integrating the Thomson heat[2] over temperature.
3. The Nernst principle (3rd law of thermodynamics) holds to the thermopower: in the limit for zero absolute temperature, the entropy and, therefore, the thermopower are zero.
4. One can build heat engines with thermopower, either to generate power from heat or to operate as cooling/refrigeration cycles. The latter cycle is what this article is about.

Figure 1a shows a thermoelectric Peltier cooler that consists of two thermoelectric semiconductors: one is doped n-type in which the majority carriers are electrons, and the thermopower and Peltier coefficients are negative ($\alpha_N < 0$, $\Pi_N < 0$), and other one is doped p-type in which the majority carriers are holes, and the thermopower $\alpha_P > 0$ and Peltier coefficient $\Pi_P > 0$. These semiconductor elements are connected in a thermopile: the electrical contacts are connected in series, as shown in Fig. 1a. An electrical power source I is attached on the hot side between the n and p-type semiconductors. This creates a heat current through each of the elements, which in turn cools down one contact to a cold-side temperature T_C, and heats up the other contacts to a hot-side temperature T_H. Assume further that α_P and α_N are not temperature-dependent between T_H and T_C. Looking at Fig. 1a from the point of view of one electron, starting from the bottom left (hot-side at temperature T_H, n-type), as that electron rises in the structure, its temperature decreases at constant value of α_N, i.e. isentropically at entropy $S_N = \alpha_N e$, under Callen's condition that the process were reversible. That progress can be followed in the (T,S) diagram (Fig. 1b). The electron then reaches the top, cold plate, where it exerts its cooling action and extracts an amount of heat Q, the cooling capacity. In that cold plate, it moves over from left to right isothermally at T_C, as can be followed in **Figure 1b**. It then heats back up to T_H in the p-type semiconductor, another isentropic transformation, at a constant entropy $S_P = \alpha_P e$, again assuming the process is considered reversible. Finally, it is pumped by the power supply I isothermally, again at the temperature T_H. Therefore, in reversible thermodynamics, a thermoelectric cooler as shown in Fig. 1a would have a thermodynamic cycle as shown in Fig. 1b. This is called a Carnot cycle, and the efficiency would be the Carnot coefficient of performance

$$COP = COP_C = \frac{T_C}{T_H - T_C} \quad (1).$$

Just like Stirling cycles with internal heat exchangers, under the (rather strong) assumption that irreversible losses are absent, Peltier coolers have a Carnot COP. Clearly, none of these assertions are true, because the losses in Peltier coolers are dominated by two main sources of irreversibility:

1. Heat is lost by thermal conduction in the semiconductors. This loss is quantified by the thermal conductivity of the materials (κ_N and κ_P), and

2. Joule heating due to the internal resistance of the thermopile though which the electrical current must pass in order to do electrical work in the load. Joule heating is minimized by maximizing the electrical conductivity σ of each of the semiconductors.

It is Altenkirch[3] who first quantified the role of these irreversibilities, and related the efficiency of the Peltier cooler in Fig. 1 to the thermoelectric figure of merit zT of each of the two semiconductors. This is defined by:

$$zT \equiv \frac{\alpha^2 \sigma}{\kappa} T \tag{2}.$$

The zT must be characterized separately for the n and p-type materials, but for simplicity we will assume that they are equal and omit the indices (or, to a first approximation, assume that for the device zT is the average between zT_N and zT_P). If so, the coefficient of performance is shown as a function of zT in **Figure 2**. We also define the thermoelectric power factor PF:

$$PF \equiv \alpha^2 \sigma \tag{3}.$$

The PF, which appears in the numerator of zT, is a measure of how much electrical power per unit volume of material a generator can produce under a constant temperature difference. Indeed, under a given $(T_H - T_C)$, α determines the voltage, $\alpha\sigma$ the current density, and the product of the two the power density.

3. CHALLENGES

The main difficulty in thermoelectric research is that α, σ, and κ are interrelated and almost mutually counter-indicated in the way they enter (2). Yet, they have to be optimized on the same material. To illustrate this, one can re-write the zT recalling that the electrical conductivity is a function of the density of charge carriers n and their mobility μ, and by recalling that the thermal conductivity is due to contributions of κ_E from the electrons and κ_L from the lattice vibrations or phonons:

$$zT = \left(\alpha^2 n\right)\left(\frac{\mu}{\kappa_E + \kappa_L}\right) eT \tag{4}.$$

The factor $(\alpha^2 n)$ in Eq. (4) contains two mutually counter-indicated properties α and n. Indeed, the thermoelectric power decreases as the charge carrier concentration increases in most solids, a relation attributed to Pisarenko[4] and shown in **Figure 3**. As a result, the power factor has a maximum at the optimal charge carrier concentration n_{OPT}, typically between 1×10^{18} cm^{-3} for solids with an electron effective mass m^* below 0.1 m_e (the free electron mass) to 5×10^{20} cm^{-3} for solids with $m^* > m_e$. In the more common thermoelectric semiconductors with $0.25\ m_e \leq m^* \leq 0.7\ m_e$, we have 2×10^{19} cm^{-3} $\leq n_{OPT} \leq 7 \times 10^{19}$ cm^{-3}. Further, the higher the value of the density of states effective mass m^*, the higher the value of the optimum power factor. This illustrates the best way maximize $(\alpha^2 n)$: select solids with high effective masses.

The factor $\mu / (\kappa_E + \kappa_L)$ in Eq. (4) contains another two other mutually counter-indicated properties μ and κ_L. Indeed, adding defects to the system to decrease the thermal conductivities of either electrons or phonons usually also decreases the electron mobility. To illustrate how to maximize $\mu / (\kappa_E + \kappa_L)$, we re-write Eq. (4), making use of the Wiedemann-Franz law that relates κ_E and σ

$$\kappa_E = LT\sigma \tag{5}.$$

where L is the Lorentz ratio. For free electrons, $L = L_0$, a smattering of universal constants giving $L_0 \equiv 2.4 \times 10^{-8}$ V^{2}K^{-2}. In practice, L varies little from L_0, and is typically $0.6\ L_0 < L < 1.4\ L_0$. Substituting this in (2) gives:

$$ZT = \frac{\alpha^2}{L} \frac{T}{1 + \frac{\kappa_L}{\kappa_E}} \quad (6).$$

This illustrates that thermoelectrics research must aim at reducing the lattice thermal conductivity, not necessarily in absolute numbers, but with regards to the electronic thermal conductivity. It also illustrates the importance of maximizing the thermopower α as long as the electrical conductivity is high enough. In the extreme case of very highly conducting metals, where the fraction of the heat carried by the phonons is zero ($\kappa_L = 0$), $zT = \alpha^2 / L$, and the primary goal of research has now shifted from optimizing zT to optimizing a single transport property, the thermoelectric power α.

Cryogenic operating temperatures add considerably to the challenges described above. Classical Peltier coolers use degenerately-doped narrow-gap semiconductors. It was recognized early[5] that the issues in thermoelectric refrigeration at cryogenic temperatures are quite different from those near ambient temperature. The most obvious problem is the factor T in zT. In addition, as the temperature decreases, the lattice thermal conductivity also increases as phonon-phonon scattering diminishes, and the diffusion thermopower decreases. *Cryogenic Peltier cooling is a challenging problem because zT decreases strongly with temperature in degenerately-doped semiconductors, following a* $zT \propto T^{5/2}$ *to* $T^{7/2}$ *law.*[6] The physical origin of the $zT \sim T^{7/2}$ law goes as follows. The first factor is of course the T in zT. Secondly, in metals and degenerately-doped semiconductors, $\alpha \sim T$ which results in a T^2 factor. The electrical conductivity follows generally a $\sigma \sim T^{1/2}$ law, when the charge carrier concentration is temperature-independent and the electrons are dominantly scattered by acoustic phonons with a scattering rate $\tau^{-1} \sim T^{1/2}$. Assuming that the thermal conductivity is dominated by phonons, and that the temperature is not so low that phonon propagation is ballistic, but rather dominated by phonon-phonon interactions, then $\kappa \approx \kappa_L \sim T^{1}$. Combining these exponents, this results in $zT \sim T^{7/2}$, which is verified experimentally: **Figure 4** shows the temperature-dependence of published or calculated zT values of historical material systems.

A second challenge comes from the fact that the maximum temperature difference ΔT_{MAX} than can be achieved in a single-stage Peltier cooler, such as shown in Fig. 1a, is limited to[7] $\Delta T_{MAX} = \frac{1}{2} zT_C^2$. Usually, other system-level losses in contact resistances and temperature gradients wasted across the mounting plates limit the ΔT_{MAX} that can be reached in practical devices based on thermoelectric materials that have $zT \approx 0.7$ to 1 to about 70 K when T_H is around 50 °C.[8] As a result, multistage Peltier coolers need to be built to reach cryogenic temperatures, in geometries similar to those shown in **Figure 5**. The difficulty with that geometry arises from the fact that the electrical and thermal contact resistances, the main sources of irreversible heat losses, increase with the number of stages. A back-of-the-envelope calculation shows that 11 stages would be needed even in an idealized cooler designed to reach 10 K from 300 K with a sequence of thermoelectric materials of zT=1 at each stage. While conceptually possible, this is a major technological challenge.

4. THERMOELECTRIC MATERIALS FOR CRYOGENIC PELTIER COOLERS DEVELOPED SINCE 2010

The following strategies are generally used to optimize zT.[8]

- (1) Phonon engineering to reduce lattice thermal conductivity
  - (1a) Engineering nanostructures that scatter phonons more than electrons
  - (1b) Engineering localized phonon modes (rattlers) to scatter acoustic phonons
  - (1c) Engineering and maximizing the anharmonicity of the chemical bonds to promote phonon-phonon interactions
- (2) Band structure engineering to enhance thermopower $\alpha(n)$
  - (2a) Engineering nanostructures to size-quantize electrons, using two-dimensional structures, quantum wells, quantum wires and quantum dots.
  - (2b) Engineering resonant impurities that produce similar effects in the band structure, but now in bulk solids.

(2c) Engineering spin-polarization in Kondo physics or correlated systems

(3) Add an additional optimization parameter to mitigate the problem of having to optimize counter-indicated properties of a single solid: magnetism and spin physics.

In 2010, the AFOSR funded a MURI program aimed at developing new materials for cryogenic Peltier cooling, under grant number FA9550-10-1-0533. The work was based on the strategies outlined above, and applied to several material systems.[9]

(1) $Bi_{1-x}Sb_x$ alloys, very narrow-gap semiconductors, were the *n*-type materials that had the best $zT \leq 0.5$ in the cryogenic range at the onset of the program; whereas the best n-type materials ear room temperature are tetradymites.[8] The tetradymite semiconductors, of the general formula $(Bi_{1-x}Sb_x)_2(Te_{1-y}Se_y)_3$, are used in commercial Peltier coolers, and in the six-stage Peltier coolers that reach the lowest cryogenic temperatures to date (about 180 K).

(2) The best p-type materials near room temperature are also tetradymites,[8] but at cryogenic temperatures below 150 K they reached $zT \leq 0.08$ at the onset of the program.[10]

(3) Heavy Fermion metals.[11],[12]

(4) Semiconductors with transition metal atoms as principal constituents, initially $FeSb_2$.[13]

During the course of the MURI program, much progress was made with all of these materials. A list of publications is available from the corresponding author upon request. For the sake of brevity, we report here only the results on the n- and p-type materials that have resulted in the highest values of *zT*.

4.1 n-type materials: $Bi_{1-x}Sb_x$ alloys

Both Bi and Sb are semimetals. They have an equal amount of electrons and holes; since electrons have a negative thermopower and holes a positive one, the total thermopower of the semimetals is small because it is the sum of the partial thermopower of electrons (negative) and holes (positive), weighted by their partial conductivities. The materials crystallize in the $\bar{3}m$ trigonal crystal structure, and the thermoelectric properties are quite anisotropic.[14] The best *zT* is achieved in elemental Bi in single crystals with heat and current fluxes aligned along the trigonal axis. The authors also calculate that, if the holes could be eliminated, the *zT* of the electrons alone in Bi would reach 1.3. This dream has never been achieved. Bi and Sb form a full range of solid solutions all with the same crystal structure as the end members. Surprisingly, the $Bi_{1-x}Sb_x$ alloys are semiconductors for $\sim 5\% \leq x \leq \sim 22\%$, even though the end members are semimetals: adding dilute amounts of Sb to Bi opens a small energy gap.[9] For $\sim 5\% \leq x \leq \sim 12\%$, single crystals of the alloys have the highest *zT* of any n-type material below about 250 K.[9] This alloy range was the starting point for the research described here.

In 2008 we discovered[15] that resonant levels could almost double the thermopower and the *zT* of p-type PbTe, with Te as the resonant impurity. The work was extended to p-type Sn-doped Bi_2Te_3.[16] The physics behind this phenomenon is reviewed in Ref [[17]]. We started a systematic search for resonant impurities in Bi, and proved that the group III elements In, Ga, and Al are indeed resonant levels in Bi, but they dope the material p-type, even though they have the same valence (3) as Bi.[18] A study of potential alkali dopants in Bi revealed that Li is a donor.[19] Here we add potassium to the list of resonant levels in Bi and $Bi_{1-x}Sb_x$ alloys, and show that it greatly increases *zT*, leading, in fact, to the record *zT*'s in the cryogenic temperature range.

A sequence of single-crystals of $Bi_{1-x}Sb_x$ alloys, with $5.5\% \leq x \leq 17\%$ was grown using a modified Bridgeman method, and doped with various amounts of K. The concentrations are all nominal, and correspond to the amount of elements put in the melt. An undoped sample of $Bi_{89.5}Sb_{10.5}$, a composition at the previously reported optimum, was grown for reference. The thermoelectric properties (thermopower α, resistivity ρ, and thermal conductivity κ) of the single-crystals were measured along the trigonal axis, and are reported in **Figure 6.** One sees from the low-temperature resistivity that samples with x > 11%, even potassium-doped, are more resistive than the sample at x=10.5 %. The resistivity of the K-doped samples with x < 10% have a much lower resistivity than the reference sample, but without a decrease in thermopower. This property greatly enhances the thermoelectric power factor of the K-doped samples reported in **Figure 7** to reach values near 300 $\mu W/cm\ K^2$, which are three times higher than the highest power factor previously reported in these alloys. As a result, a "hero"-sample of $Bi_{94.5}\ Sb_{5.5}$ doped with 0.1% K reaches a $zT \approx 0.7$ near

110 K (see **Figure 7**), and has a $zT > 0.5$ at all temperatures between 60 and 300 K. Admittedly, there is only one sample with that performance, and reproducing it proved challenging, but zT values in excess of 0.5 are readily reached.

4.2 p-type materials: $CePd_2Pt$

Just below room temperature, $CsBi_4Te_6$ has the highest p-type zT,[20] which reaches 0.8 at 220 K, but the $zT < 0.3$ for $T < 120$ K. In spite of the similarity of its formula to that of the tetradymites, the material lies in a crystal class of its own, and is really unrelated to Bi_2Te_3 or, in fact, to any other class of thermoelectric materials. The best p-type materials for lower temperature operation are described next.

Heavy Fermion systems[12] have been heavily investigated because they are the metallic compounds that have the highest thermopower. Historically, the highest power factors on p-type material were achieved in $CeSn_3$, $CePd_3$, and in n-type materials $YbAl_3$. Yet the thermal conductivities of these materials are high, and the zTs relatively modest. Again under the sponsorship of the MURI, new materials have been developed that reach $zT \geq 0.3$ over the temperature range of interest. The new p-type materials are $CePd_{3-x}Pt_x$ alloys,[21] with zT values reproduced in **Figure 8.** N-type heavy Fermion materials of formula $Yb_{1-x}(Er, Lu)_xAl_3$ have been developed[22] derived from $YbAl_3$ with higher zT than previously reported, although the BiSb alloys have higher zT values. Another n-type heavy Fermion system is (Yb, La)Cu_2Si_2.[23]

5. THE ROLE OF SPIN

Very recently, spin has been added as a parameter to circumvent the difficulty inherent in thermoelectrics research; i.e., the counter-indicated nature of the design parameters σ, κ, and α. Kondo systems rely on spin-dependent scattering, but the potential of thermal spin transport is still being investigated and the present understanding and future avenues of research are reviewed in this section. For the last 6 years, the exploration of spin caloritronic[24] effects has gained larger attention as a way of developing fundamentally new means for engineering thermal effects in materials, as well as providing methods to thermally generate pure spin fluxes. The first discovery in that field was the spin-Seebeck effect, found to exist in Permalloy at Tohoku University in 2008.[25] In 2010, the group at The Ohio State University discovered[26] the effect on a magnetic semiconductor, GaMnAs, and the Tohoku group found it on a ferromagnetic insulator, yttrium-iron garnet (YIG), at the same time.[27] Up to that time, the effect was measured in a geometry now called the transverse spin-Seebeck effect (TSSE). The Tohoku group discovered a simpler geometry on which the effect could be measured, the longitudinal Spin-Seebeck effect (LSSE). Because it can be confused with a conventional Nernst effect, the LSSE can be isolated only in electrically insulating ferromagnets.[28] Much larger TSSE effects were then found in InSb[29] using spin polarization of electrons by external magnetic fields rather than via ferromagnetism. Here, the giant spin-Seebeck effect can reach values of up to 8 mV/K, rivaling and even surpassing charge-based thermoelectrics, but only at cryogenic temperatures and high magnetic fields. The operating mechanism of the LSSE is now well established[30] and outlined next.

Figure 9 shows a diagram of an LSSE measurement using a YIG/Pt structure.[24] A 7 nm-thick Pt film is evaporated on the top surface of a crystal of YIG. A temperature gradient applied to that YIG from top to bottom generates a heat flux $j_Q = j_{QP} + j_{QM}$ that consists of heat carried by phonons (j_{QP}) and by spin waves or magnons (j_{QM}). The exact distribution between the phonon and magnon conductivity was determined recently.[31] The magnon heat flux j_{QM} is directly related to the spin-flux j_S carried by the magnons[24] $j_s = \left(\hbar / k_B T \, j_{QM} \right)$. This spin flux crosses the YIG/Pt interface at the top and spin-polarizes the conduction electrons in the Pt over a very small distance near the interface (~7nm, the spin diffusion length in Pt). Indeed, spin-flip transitions in the Pt quickly re-equilibrate the distribution of the electrons in the Pt so as to restore the same density of spin-up and spin-down electrons after one spin-diffusion length. The Pt film is thin enough that the electrons are spin-polarized through most of its thickness. Spin-polarized electrons in Pt are subject to the inverse spin-Hall effect (ISHE) [24]: due to skew scattering and other intrinsic effects, in solids made from heavy atoms, electrons scatter at different angles depending on their spin polarization. If there are more spin-up than spin-down electrons, the excess electrons accumulate on one side of the sample, creating an electric field proportional to the flux of spin-polarized electrons, which is equal to the spin flux. This is the inverse spin-Hall field $\boldsymbol{E}_{ISHE} = D\left(\boldsymbol{j}_S \times \boldsymbol{\sigma}\right)$, where, in vector notation, $\boldsymbol{j}_S$ is the vector of spin flux (which, as we have seen above is thermally driven) and $\boldsymbol{\sigma}$ is the spin polarization vector (parallel to the applied magnetic field **H**). **Figure 9** shows the orientations

of all these vectors. The end result is that a voltage appears across the Pt when a temperature gradient is applied to the ferromagnet, just like in a conventional thermoelectric, or, more precisely, like in a Nernst effect measurement (the Nernst field, like $\mathbf{E_{ISHE}}$ are perpendicular to the temperature gradient. While it has been shown[29] in InSb that the field to temperature gradient ratio (the spin-Seebeck coefficient) can be as large as for classical thermopower effects, calculations[32] of the zT of the YIG/Pt system is very poor (10^{-3}). The causes are reviewed here, as well as avenues of ongoing research.

The two main steps for the energy conversion is the transformation of the heat flux into a spin flux, and then the spin flux into a charge flux and voltage. The first step is similar to the case of classical thermoelectrics: the heat carried by electrons or magnons is equivalent to a charge or spin flux, both of which are useful, but the heat carried by phonons (the lattice) is a pure loss. Next, there are three loss mechanisms specific to the LSSE, and further research could prove that all three may be circumvented. First, the spin flux must cross the ferromagnet/metal interface, which is characterized by a parameter called the spin-mixing conductance ($g_{\uparrow\downarrow}$). This parameter is very well characterized.[33] Its physics is based on the interactions between the conduction electrons in the Pt and the core d-electrons on the ferromagnetic atoms in the YIG. It is quite akin to the mechanisms that limit the electrical resistivity of transition metals like Fe, where conduction electrons interact with core d-electrons. The fact that this mechanism leads to a resistivity that is 10 to 100 times higher in transition metals than in copper proves that this is very efficient. While $g_{\uparrow\downarrow}$ depends on the quality of the interface, generally it is not a major cause of loss of spin polarization. The second loss is the conversion of spin flux into a voltage, i.e. the efficiency of the inverse spin Hall effect. A review of this effect is given by Hoffmann.[34] From an engineering perspective, the conversion efficiency – included in the parameter D in the formula above – is at most 1% to 3% except in some narrow-gap semiconductors (InSb), which are not well studied yet. This is loss is specific to LSSE. The third, and by far the worst, loss mechanism in the LSSE is the fact that only a very small fraction of the volume of the ferromagnet contributes to the LSSE. This was proven by Kehlberger et al.[35], who measured the LSSE as in **Figure 9**, but using films of YIG grown on a non-magnetic substrate (a gadolinium gallium garnet, GGG). They plotted the spin-Seebeck coefficient as a function of YIG film thickness, and showed that the intensity of the effect increased with film thickness up to about 150 nm and saturated thereafter. This proves that only the spin flux generated in the 150 nm layer under the Pt gets converted into electrical energy. Because the temperature gradient is applied across the entire film plus substrate thickness (0.5 mm), only 0.03% of that gradient does any useful work. This is the worst energy loss mechanism, but also the easiest to address: one could make multilayers of 100 nm YIG / 7 nm Pt[36] – leaving the losses in the spin-Hall conversion as dominant loss mechanism. Such work is ongoing.

Finally, there is a connection between spin caloritronics and conventional thermoelectrics as pertains to metals: magnon drag. Usual metals have a thermopower limited to $|S| < 10\ \mu V\ K^{-1}$. In reality, metals used in thermocouples have values as high as $\pm 50\ \mu V\ K^{-1}$ or even higher; but even those values are not sufficient to give a good zT. One thermocouple material is iron, with $\alpha > 15\ \mu V\ K^{-1}$ at 300 K. As far back as the 1960s, this unusual behavior was speculatively interpreted as arising from a spin-based mechanism called magnon drag.[37] We now understand[38] that magnon drag is in fact a form of self-spin-Seebeck effect, where the electrons that give rise to the voltage are not in a layer adjacent to the ferromagnet, but in the ferromagnet itself. Such an effect was observed on metallic glasses[39].

6. TRANSVERSE THERMOELECTRIC DEVICES

Device-wise, we pointed out in section 3 that a Peltier cooler would need to have a number of stages about double that of existing commercial devices in order to be able to reach 10 K, because in Peltier devices the maximum temperature excursion per stage is limited to $\Delta T_{MAX} = \frac{1}{2} zT_C^2$. In spin-Seebeck devices this limit is circumvented, as, in fact, it is in Ettingshausen coolers[40] and all other forms of transverse[40] thermoelectrics. **Figure 10** shows why.

In the top frame, **Figure 10 (a)** shows the connection of a Peltier device. The defining topological feature of this connection is that the heat flux vector and the electrical current density vector are parallel to each other. The electrical contacts must be isothermal on the hot end in a Peltier cooler. If they were not, the wire that is connected to the cold end would act as the second leg of the thermocouple, and it would in fact be the zT of the contact wire that would have to enter the device equations for coefficient of performance or ΔT_{MAX}. Since wires are metals with low thermopower, their zT is close to zero, and device performance would be very much compromised. As a result, when current and heat flux vectors are parallel, one needs to have both n-type and p-type material with a high zT to construct

an effective Peltier cooler. Furthermore, in order to increase the voltage range, one needs to contact many such couples together in series electrically. Additionally, as is explained in Section 2, in order to increase the device $\Delta T_{MAX} = \frac{1}{2} z T_C^2$, one needs to connect devices thermally in series, as is done in Figure 2.

In contrast, **Figure 10 (b)** shows the topology where heat flux and current density vectors are perpendicular to each other. Now, isothermal surfaces appear at either the top or the bottom of the slab of thermoelectric material and can be used to apply electrical contacts. As a result, one needs only a material with one, single thermoelectric polarity, either n-type or p-type, but not both. As a result also, in order to increase the current, one only needs to increase the length of the contact strip and the dimension of the material along the y-direction, since the current is the integral of the current density along *y*. A higher voltage can be tolerated by the material by increasing the dimension along *x*. And, most importantly, the limitation that $\Delta T_{MAX} = \frac{1}{2} z T_C^2$ is lifted. The ΔT_{MAX} can in principle be increased at will simply by increasing the dimension of the material along *z*. In practice, this is not quite the case, and the material must be shaped in a particular way, as described by Goldsmid.[40] In principle, the cooling capacity of the device can be increased by simply increasing the volume of a single material, as explained. In practice, that too has its limitations. The most important requirement of transverse coolers is that, as with every cooling technology, the ΔT_{MAX}, the cooling capacity, and the coefficient of performance are three design parameters that are mutually counter-indicated and must be optimized as a whole. Yet, the fact that spin-Seebeck and self-spin-Seebeck (magnon-drag) devices are transverse coolers is one of their major advantages.

ACKNOWLEDGEMENT

This work is funded by AFOSR MURI "Cryogenic Peltier Cooling", Grant Number: FA9550-10-1-0533.

FIGURE CAPTIONS

Figure 1 (top) Schematic diagram of a Peltier cooler consisting of an n-type semiconductor and a p-type semiconductor connected as shown. (bottom) The thermodynamic cycle an electron goes through as it travels though the cooler in (a) represented in a (temperature, entropy) diagram which is the equivalent of a (temperature, thermopower) diagram.

Figure 2 Dependence of the coefficient of performance of a single-stage Peltier cooler in the zT and on the temperature gradient ΔT

Figure 3 The dependence of the thermopower of a solid on the electron concentration, a property known as the Pisarenko relation. Because the electrical conductivity increases with carrier concertation, roughly linearly when electron scattering is relatively insensitive to carrier concentration, the power factor $\alpha^2 \sigma$ has a maximum at an optimum value of the electron concentration. All thermoelectric materials must be optimized for this property.

Figure 4 Temperature dependence of the zT of some heritage thermoelectric materials at cryogenic temperatures. The tetradymite materials are similar to those described in Ref [8], the BiSb alloys in Ref [9]. The $zT \sim T^{7/2}$ law is illustrated schematically.

Figure 5 Schematic diagram of a three-stage Peltier cooler.

Figure 6 Temperature dependence of the thermopower α, resistivity ρ, and thermal conductivity κ of a series of single crystals of $Bi_{1-x}Sb_x$ alloys doped with various amounts of potassium. Nominal compositions and K doping levels are indicated. The properties are measured along the trigonal axis.

Figure 7 Temperature dependence of the thermoelectric power factor α^2/ρ and thermoelectric figure of merit zT along the trigonal axis of series of single crystals of $Bi_{1-x}Sb_x$ alloys doped with various amounts of potassium. Nominal compositions and K doping levels are indicated.

Figure 8 Thermoelectric figure of merit for $CePd_{3-x}Pt_x$ compounds. The dashed and solid lines show the values reported in earlier literature for $CePd_{2.7}Rh_{0.3}$ and $CePd_{2.655}Pt_{0.3}$ respectively. After Ref [21].

Figure 9 Illustration of the longitudinal spin-Seebeck effect (LSSE) geometry, a direct thermal spin injection from a magnon system in a ferromagnet (FM) into a normal metal (NM). The spin current polarizes the conduction electrons in the NM where, in the presence of spin-orbit interactions, it generates an electric field by the inverse spin Hall effect (ISHE). After Ref [24].

Figure 10 Comparison of a (a) longitudinal (Peltier) and (b) transverse (Nernst-Ettingshausen, Spin-Seebeck or Transverse Thermoelectric) cooler.

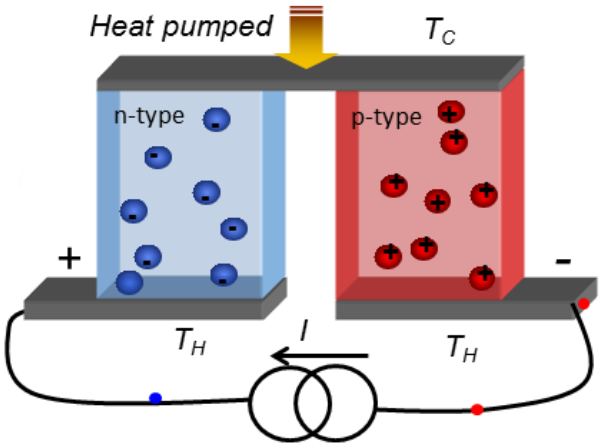

Figure 1 a

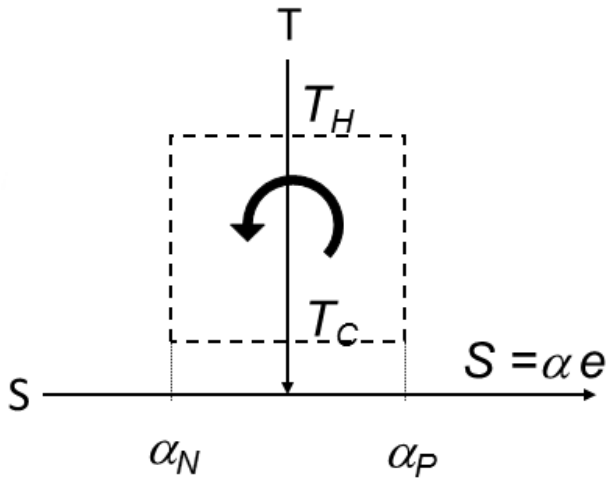

Figure 1 b

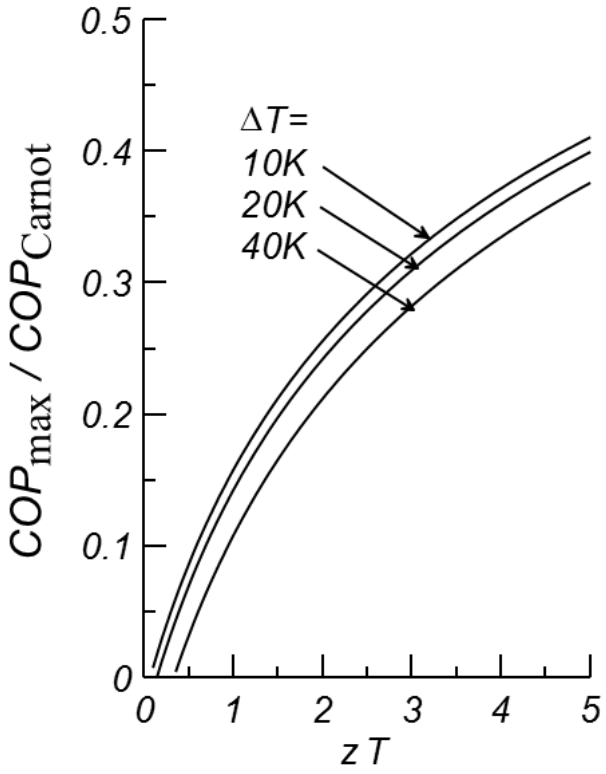

Figure 2

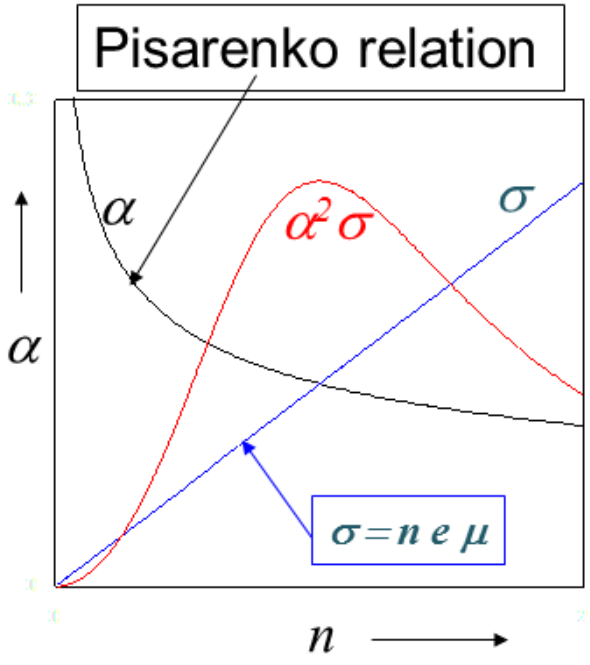

Figure 3

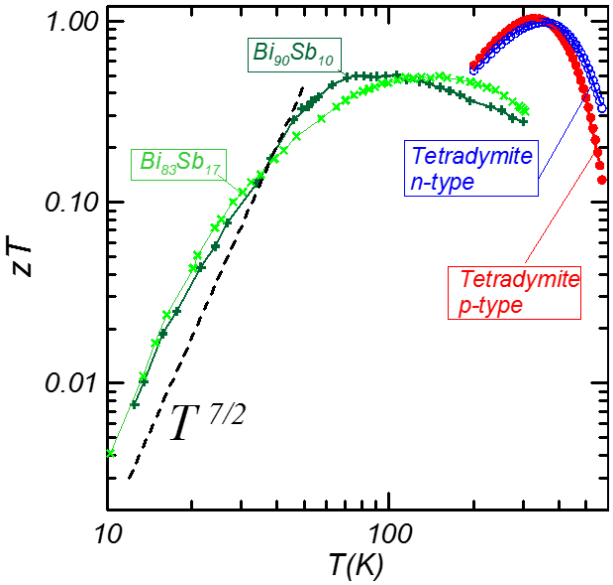

Figure 4

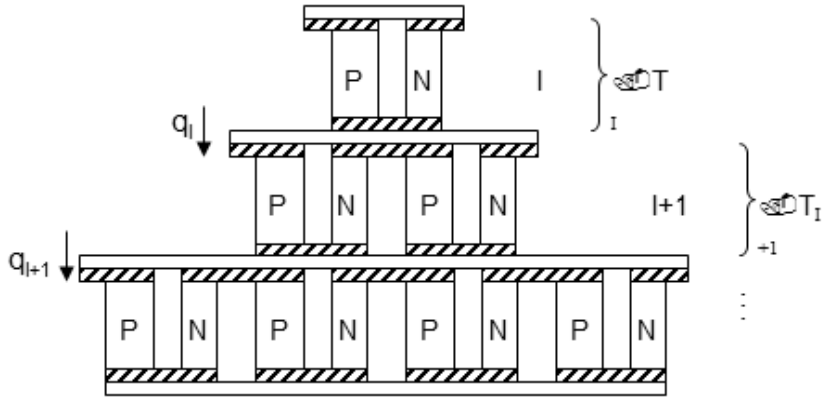

Figure 5

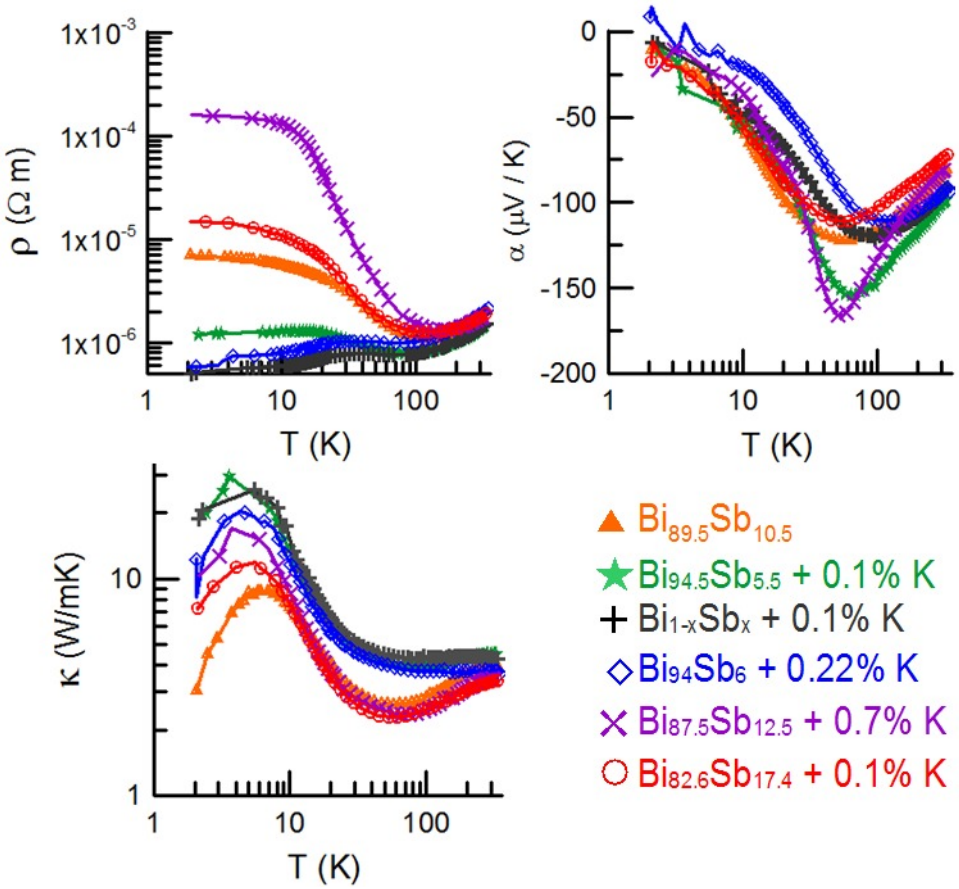
ρ (Ω m)
1x10-3
1x10-4
1x10-5
1x10-6
1
10
100
T (K)
α (μV / K)
0
-50
-100
-150
-200
1
10
100
T (K)
κ (W/mK)
10
1
1
10
100
T (K)
Bi89.5Sb10.5
Bi94.5Sb5.5 + 0.1% K
Bi1-xSbx + 0.1% K
Bi94Sb6 + 0.22% K
Bi87.5Sb12.5 + 0.7% K
Bi82.6Sb17.4 + 0.1% K

Figure 6

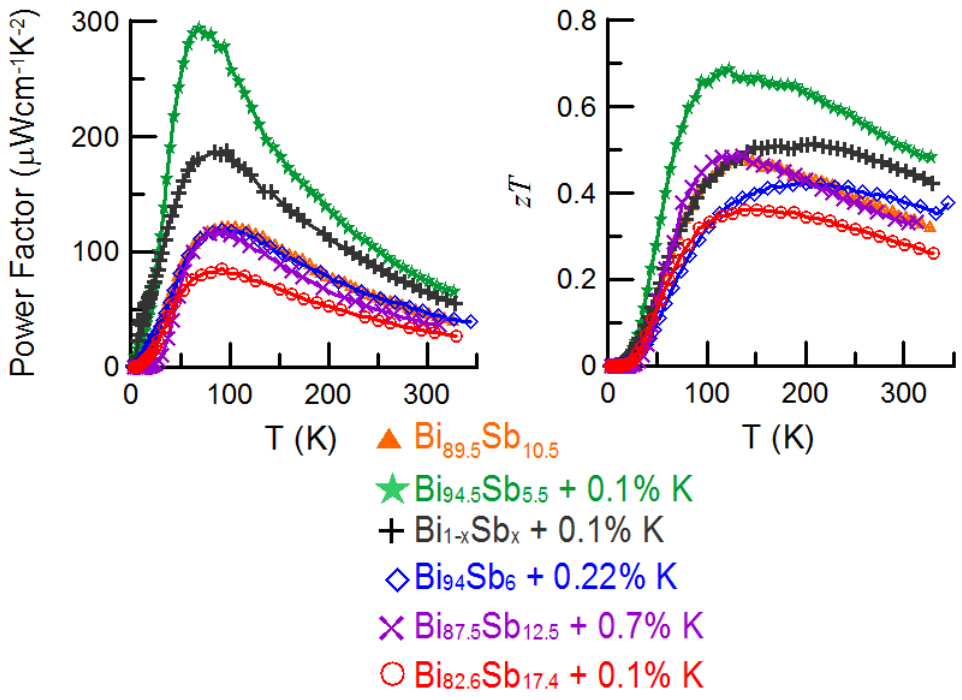
Power Factor (μWcm-1K-2)
300
200
100
0
0
100
200
300
T (K)
zT
0.8
0.6
0.4
0.2
0
0
100
200
300
T (K)
Bi89.5Sb10.5
Bi94.5Sb5.5 + 0.1% K
Bi1-xSbx + 0.1% K
Bi94Sb6 + 0.22% K
Bi87.5Sb12.5 + 0.7% K
Bi82.6Sb17.4 + 0.1% K

Figure 7

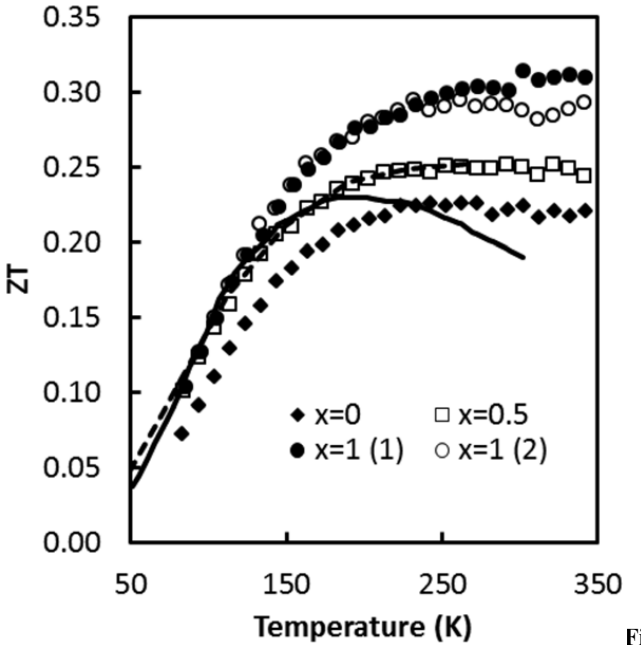

Figure 8

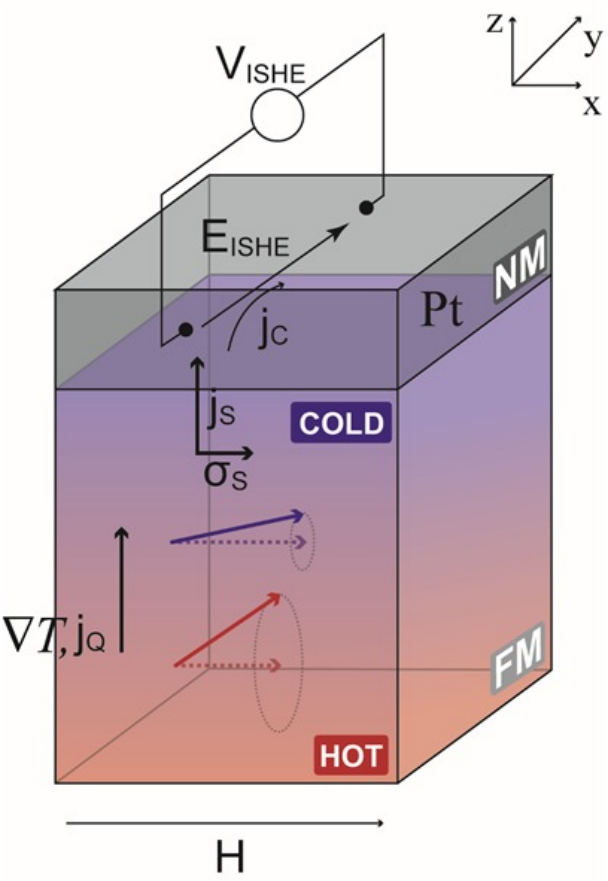

Figure 9

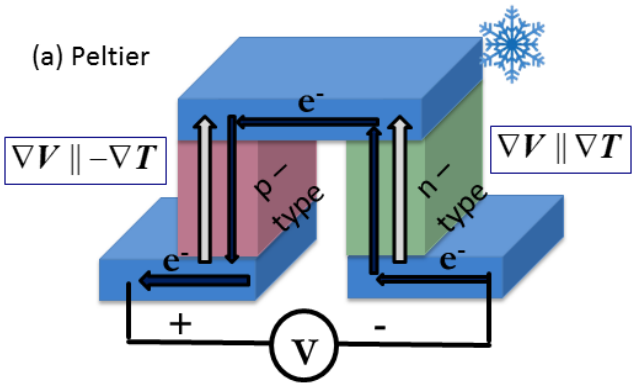

Figure 10 a

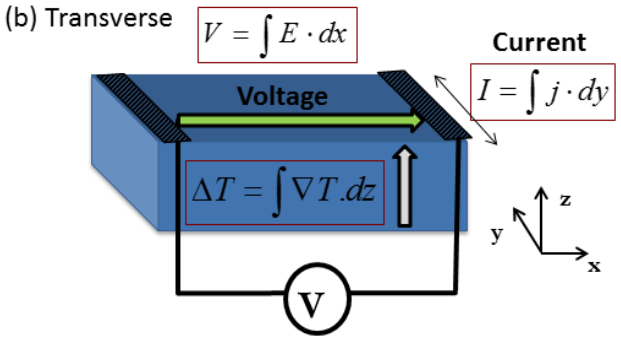

Figure 10 b

REFERENCES

[1] Callen, H. B., [Thermodynamics and an Introduction to Thermostatistics], John Wiley and Sons, New York, 1960.
[2] Roberts, R. B.. "Absolute scales for thermoelectricity," Measurement 4 (3): 101–103 (1986) doi:10.1016/0263-2241(86)90016-3; Roberts, R. B. "Absolute scale of thermoelectricity", Phil Mag 36, 91, (1977); Roberts, R. B., "Absolute scale of thermoelectricity II," Phil Mag B 43, 1123 (1981); Roberts, R. B., Righini, F. and Compton, R. C. "Absolute scale of thermoelectricity III," Phil Mag. B 52, 1147 (1985).
[3] Altenkirch, E., "Uber den Nutzeffekt der Thermosäule", Physikalische Zeitschrift 10, 560 (1909).
[4] Ioffe, A. F., [Physics of Semiconductors] Academic Press, New York, (1960).
[5] McDonald, D. K. C., Mooser, E., Pearson, W. B., Templeton, I. M., and Woods, S. B., "On the possibility of thermoelectric refrigeration at very low temperatures," Phil. Mag. 4, 433 (1959).
[6] Keyes, R. W., "Low Temperature Peltier Cooling," in [Thermoelectricity] (Heikes, R. R. and Ure, R. W., Eds.), Interscience, London, Ch. 12 (1961).
[7] Ure, R. W. and Heikes, R. R., "Theoretical calculations of device performance," in [Thermoelectricity] (Heikes, R. R. and Ure, R. W., Eds.), Interscience, London, Ch. 12 (1961).
[8] Heremans, J. P. and Wiendlocha, B., "The tetradymites: Bi_2Te_3 related materials", in [CRC Handbook on Thermoelectricity] (Uher, C., Ed.), Taylor and Francis, 2016, to be published.

[9] Lenoir, B. et al., J. Phys. Chem. Solids 59, 129 (1998).
[10] Hor, Y. S. and Cava, R. J., J. Alloys Compd. 479, 368 (2009).
[11] Mahan, G. D. and Sofo, J. O., Proc. Natl. Acad. Sci. 93, 7436 (1996).
[12] Mahan, G. D., "Good Thermoelectrics", in [Solid State Physics] (Ehrenreich, H. and Spaepen, F., Eds.), Academic Press, San Diego, vol 51, pp. 82-158, 1998.
[13] Bentien, A. et al., Europhysics Lett. 80, 17008 (2007).
[14] Gallo, C. F., Chandrasekhar, B. S., and Sutter, P. H., "Transport properties of bismuth single crystals", J. Appl. Phys. 34 144 (1963).
[15] Heremans, J. P., Jovovic, V., Toberer, E. S., Saramat, A., Kurosaki, K., Charoenphakdee, A., Yamanaka, S., and Snyder, G. J., "Enhancement of Thermoelectric Efficiency in PbTe by Distortion of the Electronic Density of States," Science 321, 554 -558 (2008).
[16] Jaworski, C. M., Kulbachinskii, V. A., and Heremans, J. P., "Tin forms a Resonant Level in Bi_2Te_3 that Enhances the Room Temperature Thermoelectric Power," Phys. Rev. B 80, 233201 (2009).
[17] Heremans, J. P., Wiendlocha, B., and Chamoire, A. M., "Resonant levels in bulk thermoelectric semiconductors," Energy Environ. Sci. 5, 5510–5530 (2012).
[18] Jin, H., Wiendlocha, B., and Heremans, J. P., "P-type doping of elemental bismuth with indium, gallium and tin: a novel doping mechanism in solids," Energ. Environ. Sci. 8, 2027-2040 (2015), (Advance Article DOI: 10.1039/C5EE01309G).
[19] Orovets, C. M., Chamoire, A. M., Jin, H., Wiendlocha, B., and Heremans, J. P., "Lithium as an interstitial donor in bismuth and bismuth-antimony alloys," J. Electronic Materials, 41, 1648-1652 (2012) (doi: 10.1007/s11664-011-1861-0).
[20] Chung, D. Y., Hogan, T., Brazis, P., Rocci-Lane, M., Kannewurf, C., Bastea, M., Uher, C., and Kanatzidis, M. G., "$CsBi_4Te_6$: A High Performance Thermoelectric Material for Low Temperature Applications," Science 287, 1024-1027 (2000).
[21] Boona, S. R. and Morelli, D. T., "Enhanced thermoelectric properties of CePd3−xPtx," Appl. Phys. Lett. 101 101909 (2012).
[22] Lehr, G. J. and Morelli, D.T., "Thermoelectric Properties of $Yb_{1-x}(Er, Lu)_xAl_3$ Solid Solutions," J. Elec. Mater. 42 (7), 1697-1701.

[23] Lehr, G. J., Morelli, D. T., Jin, H., and Heremans, J. P., "$YbCu_2Si_2$–$LaCu_2Si_2$ Solid Solutions with Enhanced Thermoelectric Power Factors," J. Elec. Mater. 44 (6), 1663-1667.

[24] Boona, S. R., Myers, R. C., and Heremans, J. P., "Spin Caloritronics," Energy Environ. Sci., 7 885-910 (2014), (DOI:10.1039/C3EE43299H).
[25] Uchida, K., Takahashi, S., Harii, K., Ieda, J., Koshibae, W., Ando, K., Maekawa, S., and Saitoh, E., "Observation of the spin Seebeck effect," Nature 455, 778-781 (2008).
[26] Jaworski, C. M., Yang, J., Mack, S., Awschalom, D. D., Heremans, J. P., and Myers, R. C., "Observation of the Spin-Seebeck Effect in a Ferromagnetic Semiconductor," Nature Materials 9 898-903 (2010).
[27] Uchida, K., Xiao, J., Adachi, H., Ohe, J., Takahashi, S., Ieda, J., Ota, T., Kajiwara, Y., Umezawa, H., Kawai, H., Bauer, G. E. W., Maekawa, S., and Saitoh, E., Nat. Mater. 9 894-897 (2010) DOI: 10.1038/NMAT2856.
[28] Uchida, K., Adachi, H., Ota, T., Nakayama, H., Maekawa, S., and Saitoh, E., "Observation of longitudinal spin-Seebeck effect in magnetic insulators," Appl. Phys. Lett. 97, 172505 (2010).
[29] Jaworski, C. M., Myers, R. C., Johnston-Halperin, E., and Heremans, J. P., "Giant spin Seebeck effect in a non-magnetic material," Nature 487, 210-213 (2012).
[30] Hoffman, S., Upadhyaya, P., and Tserkovnyak, Y., "Landau-Lifshitz theory of the longitudinal spin Seebeck effect," Phys. Rev. B 88, 064408 (2013).
[31] Boona, S. R. and Heremans, J. P., "Magnon thermal mean free path in yttrium iron garnets," Phys. Rev. B 90, 064421 (2014) (DOI: 10.1103/PhysRevB.90.064421).

[32] Kovalev, A. A. and Tserkovnyak, Y., "Magnetocaloritronic nanomachines," Solid State Communications 150, 500–504 (2010).
[33] Weiler, M.,, Althammer, M., Schreier, M., Lotze, J., Pernpeintner, M., Meyer, S., Huebl, H., Gross, R., Kamra, A., Xiao, J., Chen, Y. T., Jiao, H., Bauer, G. E. W., and Goennenwein, S. T. B., "Experimental Test of the Spin Mixing Interface Conductivity Concept," Phys. Rev. Lett. 111, 176601 (2013).
[34] Hoffmann, A., "Spin Hall Effects in Metals," IEEE Trans. Magn. 49 5172-5193 (2013).
[35] Kehlberger, A., Roser, R., Jakob, G., Klaui, M., Ritzmann, U., Hinzke, D., Nowak, U., Onbasli, M. C., Kim, D. H., Ross, C. A., Jungfleisch, M. B., and Hillebrands, B., "Determination of the origin of the spin Seebeck effect - bulk vs. interface effects," arXiv 1306.0784 (2013).
[36] Heremans, J. P. and Jaworski, C. M., "Spin Thermoelectric Generator with Multiple Magnetic Layers," Ohio State University Technology Commercialization Office, Invention disclosure T2012-251 (2012).
[37] Blatt, F. J., Flood, D. J., Rowe, V., Schroeder, P. A., and Cox, J. E., "Magnon-Drag Thermopower in Iron," Phys. Rev. Lett. 18, 395 (1967).
[38] Lucassen, M. E., Wong, C. H., Duine, R. A., and Tserkovnyak, Y., "Spin-transfer mechanism for magnon-drag thermopower," Appl. Phys. Lett. 99, 262506 (2011).
[39] Jin, H., Yang, Z., Myers, R. C., and Heremans, J. P., "Spin-Seebeck like signal in ferromagnetic bulk metallic glass without platinum contacts," Solid State Commun. 198, 40-44 (2014), http://dx.doi.org/10.1016/j.ssc.2013.12.027i.
[40] Goldsmid H. J., [Introduction to thermoelectricity], Springer-Verlag, Berlin, 2010.